



Aerodynamic analysis of uphill drafting in cycling

T. van Druenen¹ · B. Blocken^{1,2}

Accepted: 3 April 2021 / Published online: 22 April 2021
© The Author(s) 2021

Abstract

Some teams aiming for victory in a mountain stage in cycling take control in the uphill sections of the stage. While drafting, the team imposes a high speed at the front of the peloton defending their team leader from opponent's attacks. Drafting is a well-known strategy on flat or descending sections and has been studied before in this context. However, there are no systematic and extensive studies in the scientific literature on the aerodynamic effect of uphill drafting. Some studies even suggested that for gradients above 7.2% the speeds drop to 17 km/h and the air resistance can be neglected. In this paper, uphill drafting is analyzed and quantified by means of drag reductions and power reductions obtained by computational fluid dynamics simulations validated with wind tunnel measurements. It is shown that even for gradients above 7.2%, drafting can yield substantial benefits. Drafting allows cyclists to save over 7% of power on a slope of 7.5% at a speed of 6 m/s. At a speed of 8 m/s, this reduction can exceed 16%. Sensitivity analyses indicate that significant power savings can be achieved, also with varying bicycle, cyclist, road and environmental characteristics.

1 Introduction

Some teams aiming for victory in a mountain stage in cycling take control in the uphill sections of the stage. In this uphill drafting strategy, the supporting riders rotate through the front of the peloton and ride at a high pace that generally does not allow opponents to attack. There appear to be no systematic and extensive studies on the aerodynamics of uphill drafting in the literature. Most studies on cycling aerodynamics focused on the drag of a lone cyclist riding on a flat surface above 40 km/h (11.1 m/s) [1–9]. At these speeds, the aerodynamic resistance or drag is about 90% of the total resistance [1, 2, 10]. Therefore, reducing the drag of a cyclist is well known to be an important parameter for success on flat or descending sections. An efficient way to lower the aerodynamic resistance is the use of drafting. Studies on drafting were reported [11–19] in which maximum drag reductions of 48% for two cyclists [17], 57% for

four cyclists [18], 60% for nine cyclists [19], and 95% for a complete peloton [20] were found.

During uphill sections, the speeds are lower, and depending on the slope and length are generally between 20 and 30 km/h (5.5–8.5 m/s) [21]. In this case, most of the resistive force of a cyclist is due to gravitational resistance [13]. Consequently, the benefit of drafting in terms of energy saving will be lower as well. Some studies suggested that for gradients higher than 7.2%, the speeds drop to 17 km/h and the air resistance can be neglected [22]. On the contrary, Ouvrard et al. [23] demonstrated by means of field testing that drafting did have an impact on uphill cycling performances. It was found that for an uphill time trial of 2.7 km length, and a mean slope of 7.4%, the time to complete the race could be reduced by 23 s (4.2%) while drafting behind a teammate. A mean reduction in resistive force of 2.3% was found, which was mainly attributed to reduced aerodynamic drag.

The main goal of a team when maintaining a high pace in the uphill sections of a race is to protect the team leader from opponent's attacks. In this way, the team leader can maintain a constant power output, which is the most efficient strategy for long-duration cycling under constant environmental conditions [24–28]. Wilson [29] measured and estimated the power output from races and established a curve connecting the maximum recorded duration of a cyclist exerting a given power output. Taking into account that during uphill sections, the power output is already high, he found that

✉ T. van Druenen
t.v.druenen@tue.nl

¹ Building Physics and Services, Department of the Built Environment, Eindhoven University of Technology, PO Box 513, 5600 MB Eindhoven, The Netherlands

² Building Physics and Sustainable Design, Department of Civil Engineering, KU Leuven, Kasteelpark Arenberg 40, Bus 2447, 3001 Heverlee, Belgium

even a small reduction in required power, such as the 2.3% found by Ouvrard et al. [23], could extend the duration one can maintain this power [29].

To provide further insights in the potential benefits of uphill drafting, this paper presents a systematic analysis of uphill drafting by means of drag reductions and power reductions obtained by computational fluid dynamics (CFD) simulations validated with wind tunnel (WT) measurements, for pacelines of up to eight cyclists.

2 Wind tunnel measurements

The WT experiments were performed in the closed circuit WT at Eindhoven University of Technology [30]. The cross section of the WT test section is ($w \times h$) $3 \times 2 \text{ m}^2$. The cyclist models were placed on an elevated horizontal sharp-edged platform with integrated force transducer to limit the boundary layer development near the models (Fig. 1). The WT models originate from a previous study [20] and were cast from a synthetic resin (neolith) at quarter scale (frontal area = 0.03 m^2) to yield a blockage ratio of 0.7% when considering the part of the cross section above the horizontal platform. This blockage ratio is below the recommended maximum of 5% [32]. The geometry of cyclist and bicycle was obtained via 3D scanning using the Artec Eva structured light 3D scanner [31], while the cyclist (height = 1.83 m, mass = 72 kg) was asked to hold an upright position with hands on the drops, as often seen during moderate uphill sections of the race. The procedure of processing the body geometry and reporting the results was approved by the ethical board committee of Eindhoven University of Technology with reference code (ERB2020BE_1859456_WT). While in CFD the actual 3D scans were used, reinforcements and minor simplifications were applied to the wheels for manufacturing of the WT models. The wheel-to-wheel separation distance between the cyclists was 0.0375 m (full scale = 0.15 m). A force transducer, designed especially for the expected forces of quarter-scale cyclist models [20], with an accuracy of 0.001 N was used, which corresponds to a systematic error of $3 \times 10^{-6} \text{ m}^2$ for $C_D A$ (coefficient of drag times frontal surface area).

Tests were performed at quarter scale up to 25 m/s to ensure a close Reynolds number similarity with the full-scale speed of 6 m/s. During every measurement, the free stream wind speed and turbulence intensity were recorded near the cyclists by the use of a Cobra probe (Fig. 1c). The turbulence intensity at the position of the force transducer was 0.5%. Atmospheric pressure, air temperature and humidity were measured at the end of the test section. The drag force results were corrected to match 15 °C at 0 m (sea level) and standard atmospheric pressure 101,325 Pa. These conditions were also applied in the CFD simulations.

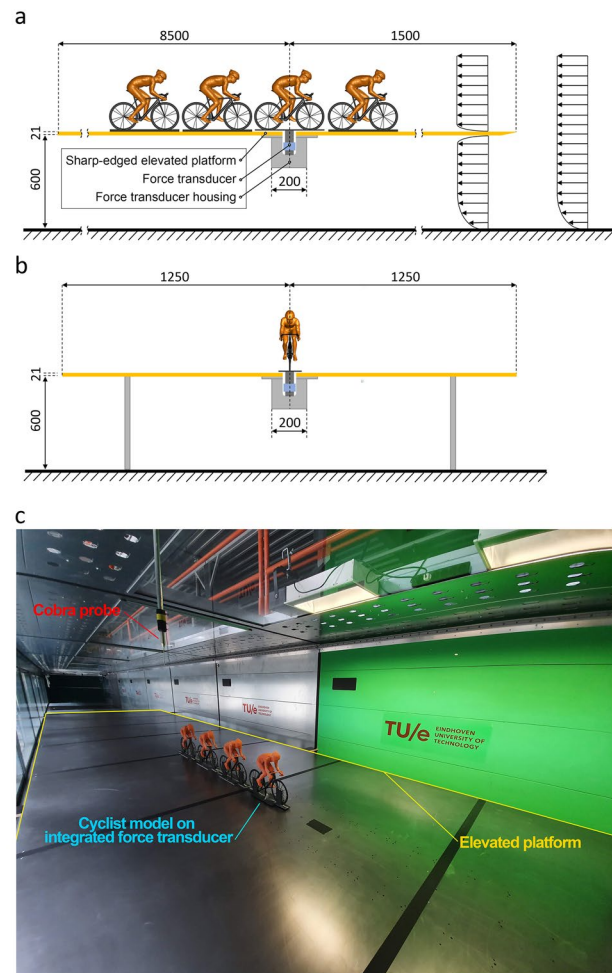


Fig. 1 Wind tunnel set-up. Dimensions in mm

3 CFD simulations

3.1 Computational geometry, domain and grid

The simulations were performed at full scale and the models were placed in a domain with size according to CFD best practice guidelines [33, 34], based on the configuration with eight cyclists. The resulting domain dimensions were ($l \times w \times h$) $54.5 \times 17.5 \times 8.75 \text{ m}^3$. Both the cyclist geometry and the hybrid hexahedral–tetrahedral computational grid topology were similar to those used before [9, 20]. Due to a lower cycling velocity in the current study, an additional grid-sensitivity analysis was performed. For the grid-sensitivity analysis, three grids were constructed for the single cyclist configuration in which surface and volume cell sizes were systematically refined (Fig. 2). This resulted in a coarse, medium and fine grid containing 26,952,545, 35,248,553 and 45,402,859 cells, respectively. Studies (e.g. Ref. [35]) highlight the importance

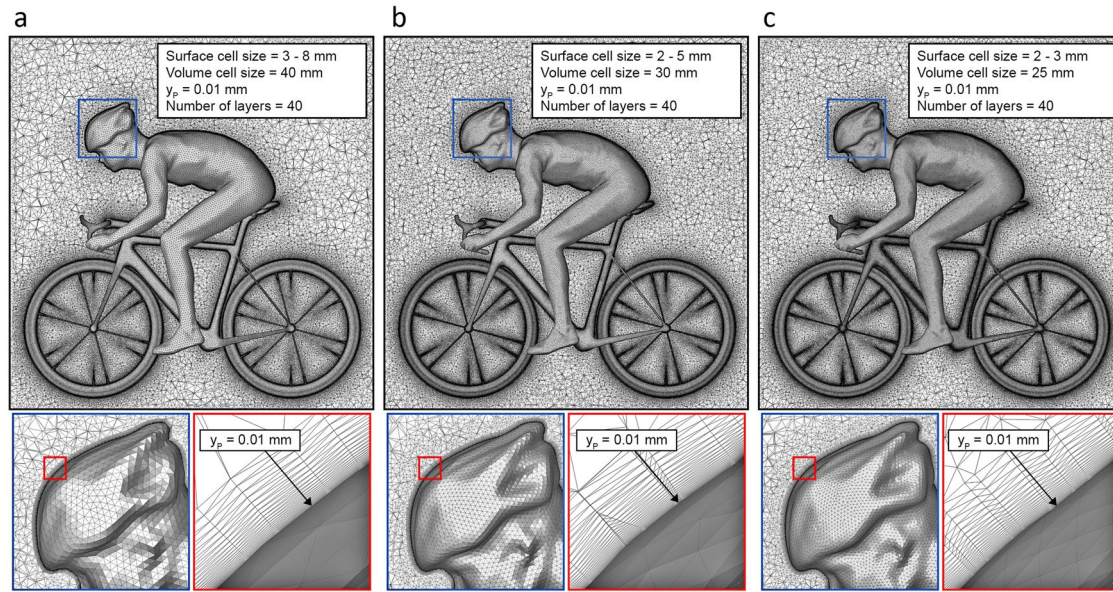


Fig. 2 Computational grid for the isolated cyclist: **a** coarse grid of 26,952,545 cells, **b** medium grid of 35,248,553 cells, and **c** fine grid of 45,402,859 cells

of keeping the dimensionless wall unit y^* below one for resolving the thin viscous sublayer to reproduce boundary layer flow and separation. The dimensionless wall unit is given by $y^* = u^*y_p/\nu$ where u^* is the friction velocity, y_p is the normal distance of the cell center point P from the wall surface and ν is the local kinematic viscosity. Based on this definition and a free stream velocity of 6 m/s, $y_p = 0.026$ mm would satisfy $y^* < 1$. However, due to flow acceleration, the local friction velocity u^* can increase, which would demand a smaller y_p to satisfy $y^* < 1$. Therefore, the choice was made to keep y_p at 0.010 mm for all three grids.

The grid-sensitivity analysis was conducted with both the Transition SST (TSST) [38, 39] and Scale-Adaptive Simulation (SAS) approach [40, 41]. The results were compared in terms of the drag area for the combined cyclist-bicycle system. In general, the drag area did not change much for the finer grids. The use of the coarse grid resulted in a difference of 0.9 and 1.7% compared to the fine grid for, respectively, the TSST (0.4988 vs. 0.4945 m²) and SAS (0.4646 vs. 0.4725 m²) approach. For both the TSST (0.4938 vs. 0.4945 m²) and SAS (0.4729 vs. 0.4725 m²) approach, the drag area obtained on the medium grid differed by 0.1% from the results on the fine grid. Therefore, the medium grid was retained for the remainder of this study.

3.2 Boundary conditions

A uniform mean velocity of 6 m/s was imposed at the inlet with a turbulence intensity of 0.5%. These conditions ensure

a similar Reynolds number to those of the quarter-scale models in the WT and represent the relative air movement due to cycling in calm conditions (zero wind speed). The bicycle surfaces were modeled as smooth no-slip walls. The cyclist body surfaces were modeled with an equivalent sand-grain roughness height of $k_s = 0.1$ mm [20, 36]. Zero static gauge pressure was specified at the outlet. The bottom, top and lateral boundaries of the domain were treated as slip walls.

3.3 Approximate form of governing equations and solver settings

The CFD simulations were performed using the commercial CFD code ANSYS Fluent 19.2 [37]. Two approaches were adopted. The first, less computationally demanding approach, consisted of solving the 3D steady Reynolds-averaged Navier–Stokes (RANS) equations with the transition shear stress transport (TSST) turbulence model for closure [38, 39]. Curvature correction was applied. Pressure–velocity coupling was taken care of by the COUPLED algorithm. Pressure interpolation was second order and second-order discretization schemes were used for both the convection and the viscous terms of the governing equations. The Green–Gauss node-based scheme was used for gradient interpolation. To avoid possible divergence of the solution due to high-pressure gradients, the simulations were conducted under pseudo-transient conditions with a pseudo time step of 0.01 s for a minimum of 10,000 pseudo-transient time steps. Averaged results were obtained by averaging over

the last 9000 time steps, after an oscillatory phase of the sampled drag values was reached.

The second approach consisted of the use of Scale-Adaptive Simulation (SAS) [40, 41], coupled with the SST $k-\omega$ model [42]. The SAS model is an improved URANS formulation which employs URANS for wall-bounded flows and allows the resolution of turbulence structures in regions of high flow instabilities. SAS methods are most promising in flows with significant instability mechanisms present, such as in the near wake of bluff bodies [40, 43]. Pressure–velocity coupling was performed by the PISO algorithm. Pressure interpolation was second order. Second-order upwind discretization schemes were used for the turbulence model equations and bounded central differencing was used for the momentum equations. Gradient interpolation was taken care of by the Green–Gauss node-based scheme. To determine a suitable time step Δt , a sensitivity analysis was performed for the single cyclist configuration. For all simulations, the Courant–Friedrichs–Lewy (CFL) number $CFL = U\Delta t/\Delta x$, with $U = 6$ m/s and $\Delta x = 0.03$ m, was kept below one in the regions between the cyclists. Compared to the smallest tested time step size $\Delta t = 0.0005$ s ($CFL = 0.1$), the use of larger time step sizes $\Delta t = 0.001$ s ($CFL = 0.2$) and $\Delta t = 0.002$ s ($CFL = 0.4$) resulted in respective differences of 0.11 and 1.47% in drag. Based on a trade-off between computation time and accuracy, the time step size of $\Delta t = 0.001$ s was retained for all SAS simulations. Results were averaged after an oscillatory phase of the sampled drag values was reached. The number of time steps required to obtain a constant moving average of the drag values ranged from 5000 to 10,000.

4 Results

4.1 CFD validation: pacelines up to four cyclists

Figure 3 shows the results from the WT measurement and CFD simulations in terms of percentage drag of that of an isolated rider at equal speed. It is shown that all riders benefit from drafting. From the WT measurements, the rider in front (C1) experienced drag reductions of 3% (Fig. 3a) and 4% (Fig. 3b, c). The reduction in drag for the following riders was larger. A maximum reduction down to 44% was found for the fourth rider (Fig. 3c). The CFD simulations show a similar trend. The results obtained by the TSST turbulence model underestimated the drag of the trailing riders by 5.1% on average. The results obtained with the SAS model deviated from the WT measurements by 1.7% on average. For this reason, the SAS approach was used for the rest of the study.

4.2 CFD simulations: pacelines up to eight cyclists

Figure 4 shows the results obtained by the SAS approach for pacelines of up to eight cyclists. The lowest drag percentage per configuration is marked in green. In line with studies on drafting cyclists [16, 19, 20, 44, 45] due to subsonic upstream disturbance, the drag on the leading cyclist decreases due to the other cyclists in its wake. The drag on the leading cyclist decreases with increasing number of cyclists up in the paceline to a maximum of 4% for configurations with five cyclists or more. In general, the drag decreases for positions further down the paceline. For configurations up to four cyclists, drag reaches a minimum for the last cyclist. For configurations of 5, 6, 7 and 8 cyclists, the second-to-last position is the position with the lowest drag. An explanation for this phenomenon is provided in

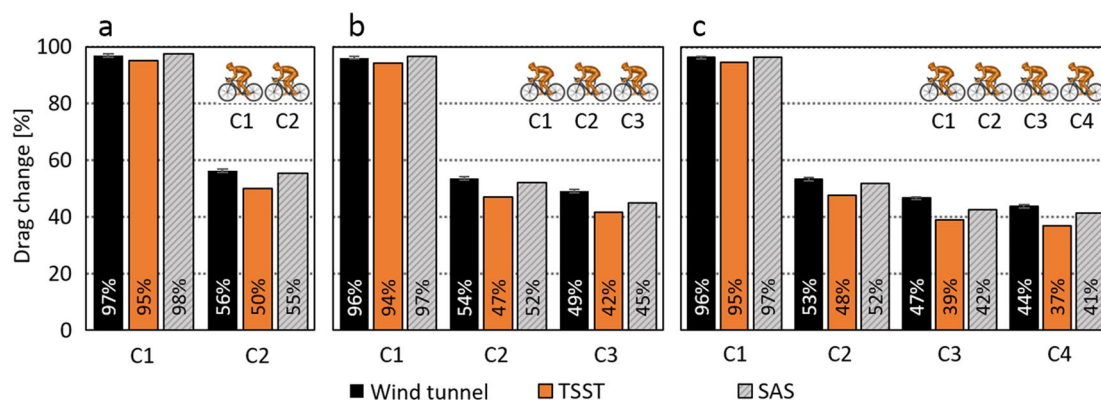


Fig. 3 Comparison of CFD and wind tunnel drag results for the **a** two, **b** three, and **c** four cyclists configuration, as a percentage of the drag of an isolated cyclist. Error bars represent the size of one standard deviation

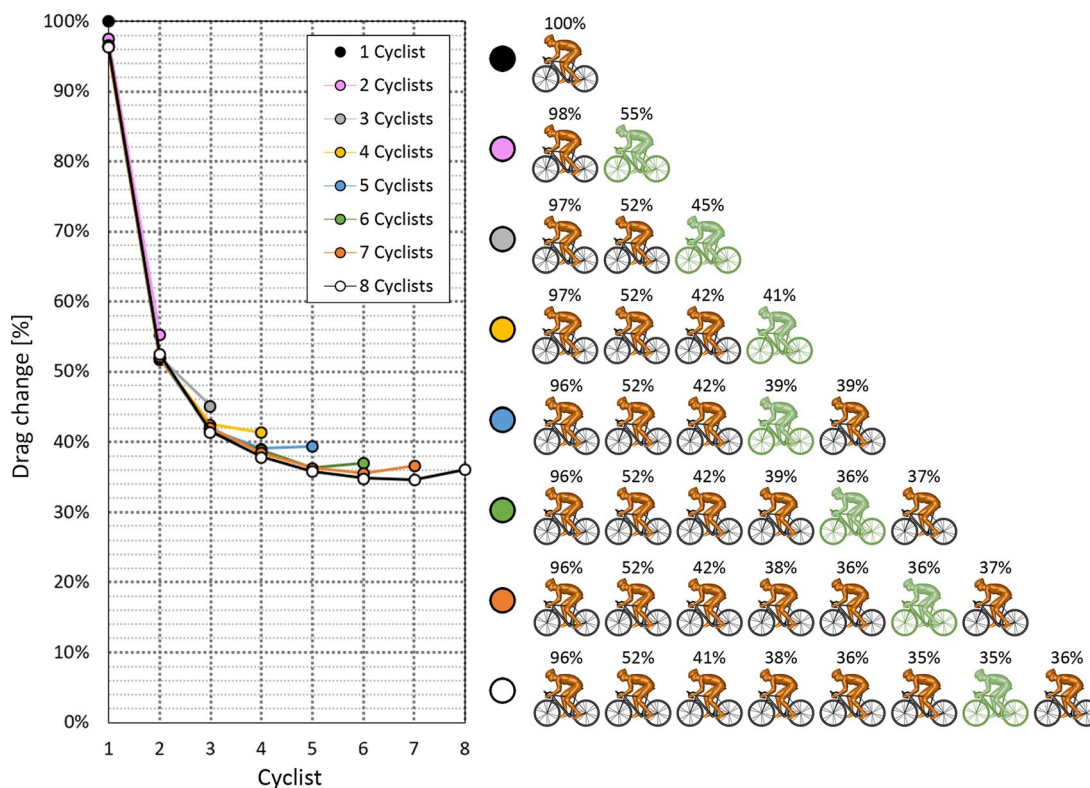


Fig. 4 Drag of every cyclist in configurations up to eight cyclists, as a percentage of the drag of the isolated cyclist. The cyclist with the lowest drag is colored in green (color figure online)

[19] and confirmed by the contours of mean velocity ratio in Fig. 5b, d, as well as by Fig. 6 which shows the cross-sectional area of the wake (mean velocity ratio < 0.5) in a vertical plane situated at the most upstream point of the front wheel. The velocity ratio is defined as the magnitude of the local 3D velocity vector divided by the cycling speed of 6 m/s. The strong expansion of the wake originating from the first cyclist continues to about position five. From this point on, the expansion of the wake flattens out and all positions further downstream have a similar benefit from drafting in this wake. Because the last cyclist does not have the benefit of someone drafting behind them, they experience more drag.

The impact of the subsonic upstream disturbance is also visible in the instantaneous (Fig. 5e, g) and mean (Fig. 5f, h) contours of the pressure coefficient. The under-pressure (blue) area behind the leading rider is decreased in size and magnitude when one or more trailing cyclists are present. The largest area of overpressure (red) is visible in front of the leading cyclist and decreases in size for the positions further to the back of the formation. This is due to the interaction with the under-pressure area behind the leading cyclist with the overpressure area in front of the trailing cyclist.

4.3 Power calculations

The ascent of the Col du Tourmalet, the most climbed mountain pass in the history of the Tour de France [46], served as a case study for calculating the required total power P_{TOT} for every cyclist in the paceline. The climb features a mean slope of 7.5%. A representative mean speed of 22 km/h (6.1 m/s) was selected based on elite cyclists' performance [21, 47]. The power model of Martin et al. [13] was used to calculate P_{TOT} required to overcome aerodynamic drag P_{AD} , rolling resistance P_{RR} , wheel bearing friction P_{WB} , ascending and descending P_{PE} , acceleration P_{KE} , and friction in the drive chain E_C :

$$P_{TOT} = \frac{P_{AD} + P_{RR} + P_{WB} + P_{PE} + P_{KE}}{E_C}$$

This study focused on riding at constant speed, so P_{KE} was zero and hence was not considered here. In still air, the power to overcome the total aerodynamic drag P_{AD} is defined by

$$P_{AD} = \frac{1}{2} \rho (C_D A + F_w) U^3$$

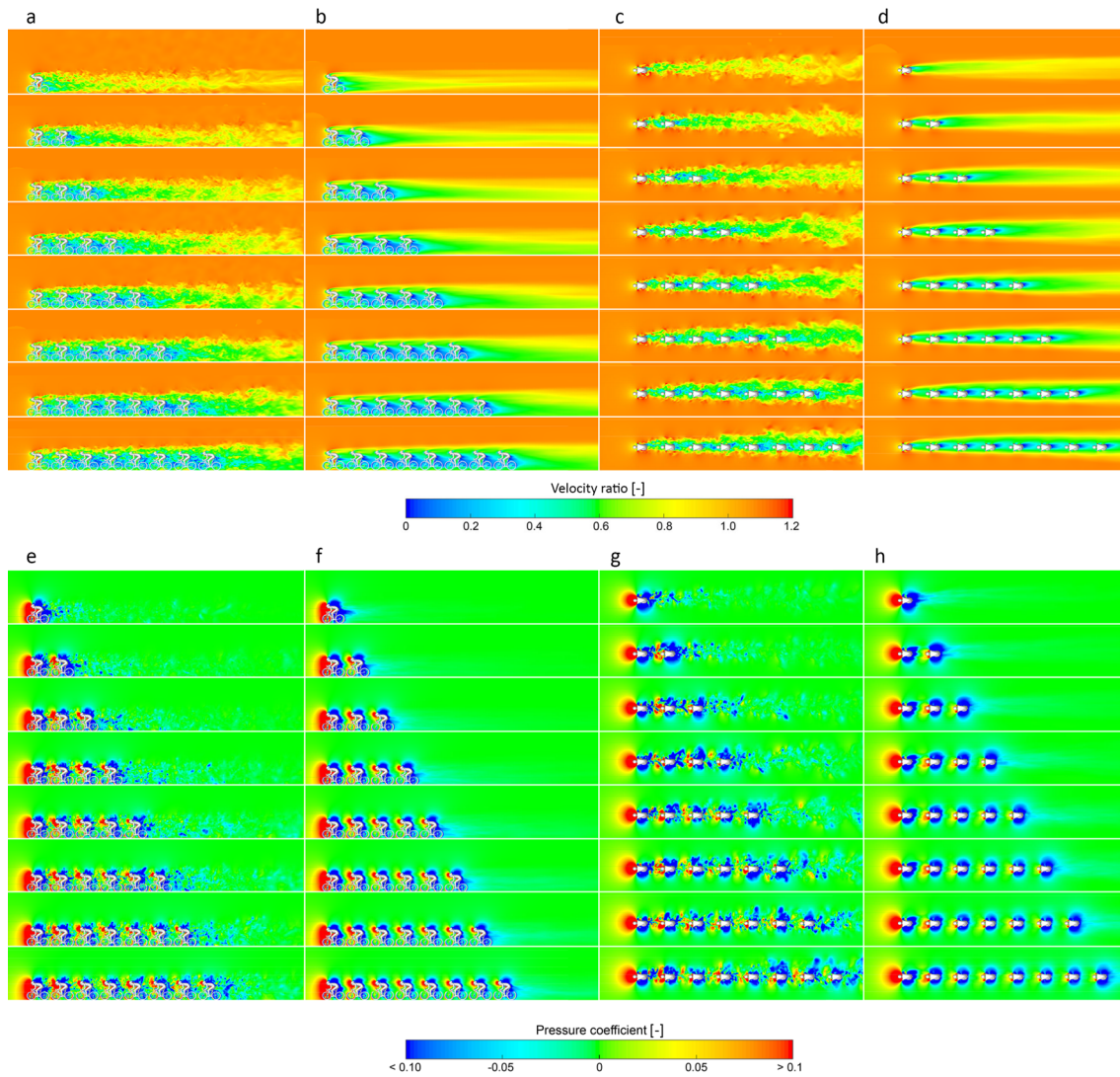


Fig. 5 Contours of **a, c, e, g** instantaneous and **b, d, f, h** mean **a, b, c, d** velocity ratio and **e, f, g, h** pressure coefficient in **a, b, e, f** vertical centerplane and in **c, d, g, h** horizontal plane at 1 m height

in which ρ is the air density (kg/m^3), C_D is the drag coefficient (-), A is the frontal area (m^2), and U is the riding speed of the cyclist (m/s). The incremental drag area of the spokes is given by F_W (m^2). The power to overcome the rolling resistance P_{RR} is described by

$$P_{RR} = UC_{RR}mg$$

where C_{RR} is the coefficient of rolling resistance (-), m is the total mass of bike and rider (kg), and g is the acceleration of gravity ($=9.81 \text{ m/s}^2$). The total power lost to bearing friction torque P_{WB} as a function of riding speed U is

$$P_{WB} = U(91 + 8.7U)10^{-3}$$

The power associated with changes in potential energy P_{PE} , due to ascending or descending for road grades of up to 10%, is related to the total mass of the bike and rider and to the road gradient G (rise/run) as

$$P_{PE} = UGmg$$

The total power P_{TOT} is calculated from a number of input parameters depending on the bicycle, cyclists, road and environmental characteristics. The input parameters, including the computed drag area values for configurations up to eight cyclists, are provided in Table 1. It was assumed that all cyclists have equal morphological characteristics and that



Fig. 6 Cross-sectional area of the wake (mean velocity ratio < 0.5) as a function of longitudinal distance for pacelines of up to eight cyclists

Table 1 Input parameters

Parameter	Symbol	Unit	Value
Riding speed	U	m/s	6
Wind speed	V	m/s	0
Rotational drag area	F_w	m ²	0.0044 [13]
Air density	P	kg/m ³	1.225
Rolling resistance coefficient	C_{rr}	–	0.0032 [13]
Mass	M	kg	72
Gravitational acceleration	g	m/s ²	9.81
Road gradient	G	%	7.5
Efficiency of drive train	E_C	%	98
Drag area			
1 cyclist configuration	C_{DA}	m ²	0.473
2 cyclists configuration	C_{DA}	m ²	0.461, 0.261
3 cyclists configuration	C_{DA}	m ²	0.457, 0.246, 0.213
4 cyclists configuration	C_{DA}	m ²	0.457, 0.246, 0.201, 0.196
5 cyclists configuration	C_{DA}	m ²	0.454, 0.246, 0.198, 0.185, 0.186
6 cyclists configuration	C_{DA}	m ²	0.454, 0.246, 0.196, 0.184, 0.172, 0.175
7 cyclists configuration	C_{DA}	m ²	0.454, 0.246, 0.196, 0.182, 0.172, 0.168, 0.173
8 cyclists configuration	C_{DA}	m ²	0.454, 0.246, 0.196, 0.179, 0.170, 0.165, 0.164, 0.171

their C_{DA} is invariant with speed. Standard atmospheric conditions were applied.

Figure 7a presents the required power for the isolated cyclist to overcome a slope of 7.5% as a function of cycling speed, with the different power components indicated. Figure 7b shows the cumulative power percentage. Changes in potential energy had the largest contribution to the total power. With a speed of 6 m/s, 80.2% of P_{TOT} is required for P_{PE} , 16.2% for P_{AD} and 3.4 and 0.2% for P_{RR} and P_{WB} , respectively. Every required power component increases with increasing speed.

Figure 8 shows P_{Req} per cyclist to overcome a slope of 7.5%, as a function of speed. P_{Req} is defined as the required P_{TOT} per cyclist, expressed as percentage of the

required P_{TOT} for an isolated cyclist. The leading (first) cyclist had a small benefit compared to the isolated cyclist. Larger benefits were found for the trailing cyclists. For two cyclists at 6 m/s, the second one needed 7.1% less power than the isolated cyclist. For pacelines of three to eight cyclists, this reduction was 7.6% (Fig. 8b–g). At 6 m/s, the reduction in P_{Req} for the third cyclist was 8.7% for a paceline with three (Fig. 8b), 9.1% for a paceline with four (Fig. 8c), and grew to 9.3% for a paceline with eight cyclists (Fig. 8g). These drag reduction benefits increased with increasing speed. For a paceline with eight cyclists at 8 m/s, the benefit for the second and third cyclist was about 12 and 14%, respectively, while reductions in P_{Req}

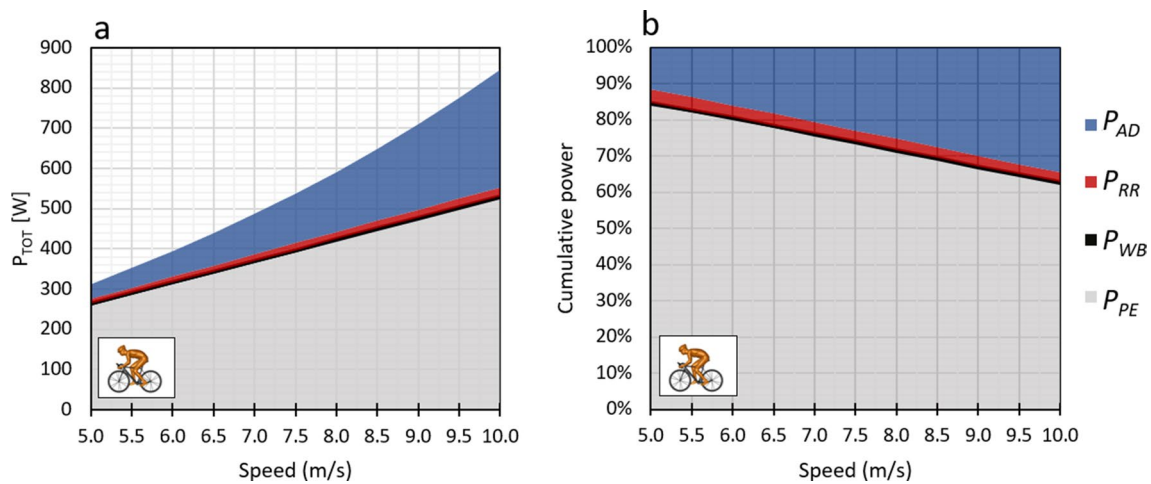


Fig. 7 **a** Power as the sum of components P_{AD} , P_{RR} , P_{WB} , and P_{PE} and **b** cumulative power percentage required to overcome a slope of 7.5% as a function of speed for the isolated cyclist

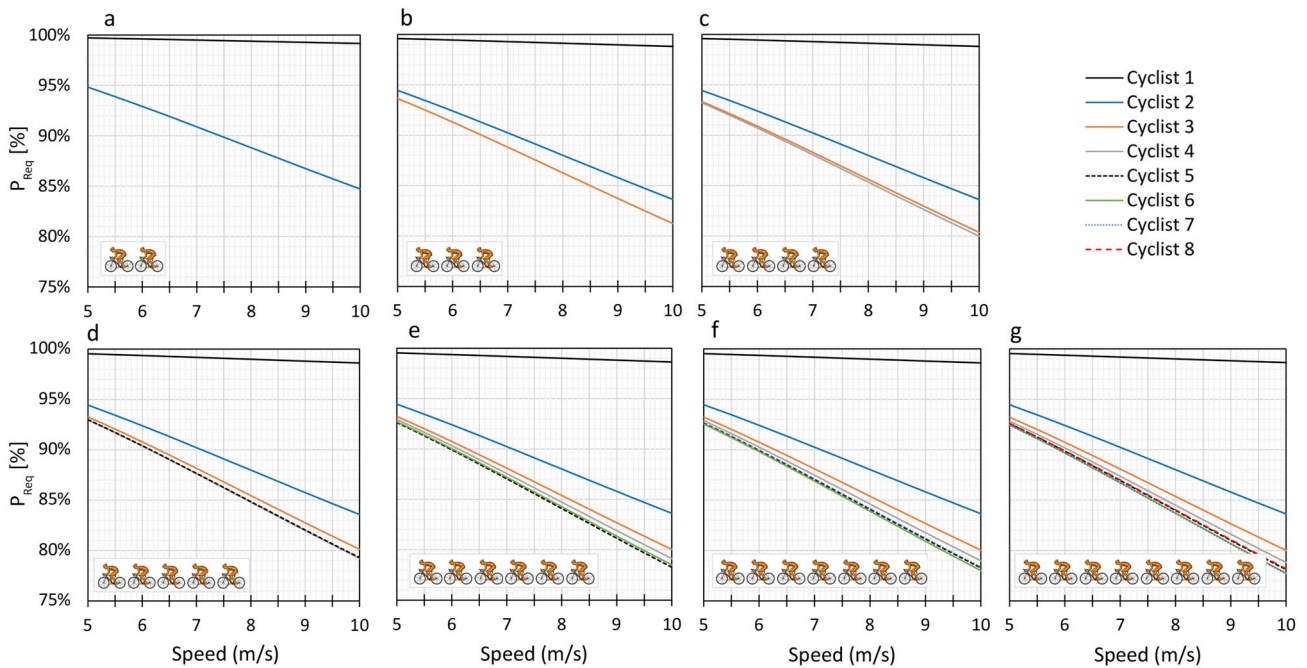


Fig. 8 Required total power P_{Req} as a function of speed to overcome a slope of 7.5%, expressed as a percentage of the power of an isolated cyclist, for the **a** two, **b** three, **c** four, **d** five, **e** six, **f** seven, and **g** 8 cyclists configuration

of about 16 and 20% were found at 10 m/s. For the cyclists further down the paceline, this grew to values of about 22%, with a maximum reduction of 22.4% for the seventh cyclist.

A sensitivity analysis was performed concerning the impact of the main input values on the results (Fig. 9 and Table 1). Results were evaluated in terms of P_{Req} . For the sake of brevity, only the configurations of up to four cyclists were included. With respect to P_{Req} , positive

relationships were found for m and G , while negative relationships were found for ρ , U and C_{DA} . Changing the input values had little effect on P_{Req} for the leading cyclist (Fig. 9a, c, f). Increasing or decreasing one of the input parameters by 20% yielded a maximum change of 0.1%. Larger changes were found for the trailing cyclists. If the combined mass of cyclists and bicycles increased by 20% for the two cyclists configuration, and the other parameters did not change, the reduction in P_{Req} was about

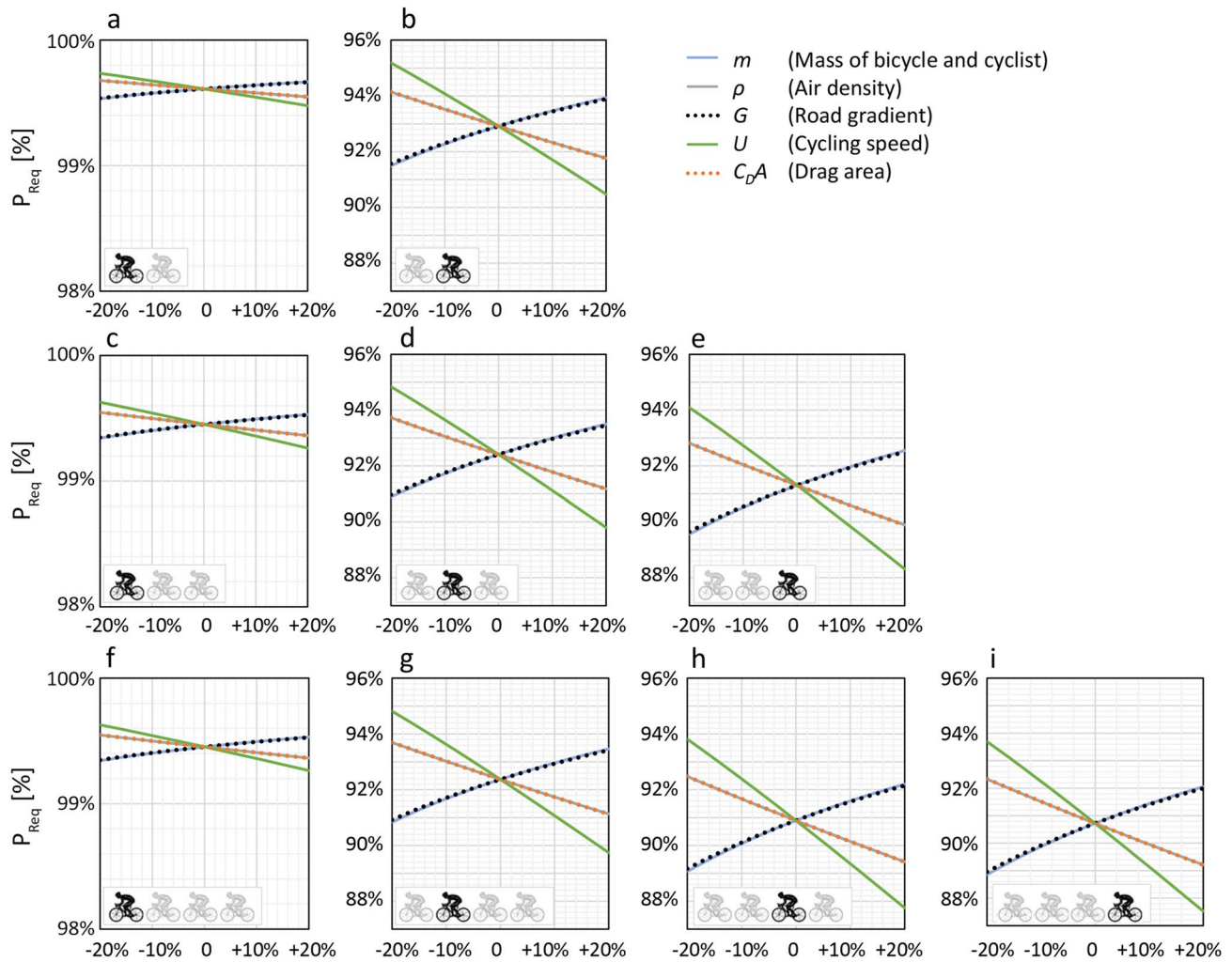


Fig. 9 Sensitivity analysis of the impact of several input parameters on the required power P_{Req} for every cyclist. This for the **a, c, f** first, **b, d, g** second, **e, h** third and **i** fourth cyclist in **a, b** two, **c, d, e** three,

and **f, g, h, i** four cyclists configuration. Initial input parameters are given in Table 1

1% (Fig. 9b). For the other cyclists in second (Fig. 9d, g), third (Fig. 9e, h) and fourth (Fig. 9i) position, values up to 1.2% were found. Comparable results existed for G . The negative relationships for ρ and $C_D A$ were of the same magnitude as those found for the positive relationships. Increasing one of these parameters by 20% yielded further reductions of P_{Req} in the range of 1 and 1.3% for the trailing cyclists. The sensitivity to speed was already highlighted in Fig. 8 and was demonstrated again here. With additional reductions up to 3.1% (Fig. 9h) for an increase of 20%, the sensitivity to speed was larger than for the other parameters.

5 Discussion

Using the uphill drafting strategy a team can try to keep their opponents from attacking while making sure their team leader can maintain a constant power output and does not have to spend energy in countering attacks. Uphill drafting is favorable for cyclists who can maintain a high power output with respect to their weight (W/kg) for a long duration. As shown in Sect. 4.3, drafting at 6 m/s under the given circumstances can reduce the required power by about 7% for the second cyclist and up to 10% for the other cyclists in line. Considering the power output of elite cyclists during uphill sections is in the range of 300–400 W [21] and the relation between power output and duration by Wilson [29] (see Sect. 1), it is expected that power reductions in the range of 5–10% could extend the duration of this power

output up to about 15 min. Future research could incorporate elite cyclists power output data during uphill performances, to better determine the actual time gain and adjust the uphill strategy accordingly.

Competitors can also use the wake drawn by other teams to benefit from drag and power reductions. However, when a team applies the uphill drafting strategy, they are generally convinced that their leader is the strongest cyclist in terms of power-to-weight ratio or that they can defend the time gains they can take in other stages (e.g. time trial stages). Other potential benefits are related to the psychophysiological part of cycling. Pleasure and positivity allow the cyclist to sustain higher exercise intensity [48–50]. It is suggested that the presence and leading roles of teammates increases positivity [23], increasing power output for the team leader.

The study was subjected to a number of limitations. Crosswind effects were not taken into account. The bicycle wheels did not rotate, the cyclists were not pedaling and all cyclists had equal body characteristics. In addition, in Sect. 4.3 it was assumed that the C_{DA} remains constant with increasing cycling speed. While the effect of speed on C_{DA} should be the subject of future work, it is expected that the impact of most of these limitations was well captured within the range of $\pm 20\%$, as applied in the sensitivity analysis (Sect. 4.3).

6 Conclusion

While uphill drafting is a common strategy in mountain stages in cycling, its effect is questioned and there are no systematic and extensive studies in the scientific literature on this topic. Therefore, this study presents an aerodynamic analysis on uphill drafting in cycling by means of WT measurements and CFD simulations. Drag reductions were computed and a power model was used to calculate potential power savings. For configurations of up to four cyclists, the last rider experienced the lowest drag. For configurations of five to eight cyclists, the second-to-last cyclist experienced the lowest drag. By drafting on a slope of 7.5% at a speed of 6 m/s, cyclists can save over 7% in terms of the required power. At higher speeds of 8 m/s, savings of over 12% can be achieved. Under the given conditions, the largest differences in required power are found between the cyclists in first, second and third positions. Comparable power reductions are found for all remaining cyclists in the paceline. The sensitivity analysis of input variables shows that uphill drafting allows power savings with different bicycle, cyclist, road and environmental characteristics.

Supplementary Information The online version contains supplementary material available at <https://doi.org/10.1007/s12283-021-00345-2>.

Acknowledgements The authors acknowledge the partnership with ANSYS CFD. This work was carried out on the Dutch national e-infrastructure with the support of SURF Cooperative.

Declarations

Conflict of interest The authors declare that they have no conflict of interest. The second author is an associate editor of the journal and was not involved in the double-blind peer-review process.

Open Access This article is licensed under a Creative Commons Attribution 4.0 International License, which permits use, sharing, adaptation, distribution and reproduction in any medium or format, as long as you give appropriate credit to the original author(s) and the source, provide a link to the Creative Commons licence, and indicate if changes were made. The images or other third party material in this article are included in the article's Creative Commons licence, unless indicated otherwise in a credit line to the material. If material is not included in the article's Creative Commons licence and your intended use is not permitted by statutory regulation or exceeds the permitted use, you will need to obtain permission directly from the copyright holder. To view a copy of this licence, visit <http://creativecommons.org/licenses/by/4.0/>.

References

1. Kyle CR, Burke ER (1984) Improving the racing bicycle. *Mech Eng* 106(9):34–45
2. Grappe G, Candau R, Belli A, Rouillon JD (1997) Aerodynamic drag in field cycling with special reference to the Obree's position. *Ergonomics* 40(12):1299–1311
3. Padilla S, Mujika I, Angulo F, Goiriena JJ (2000) Scientific approach to the 1-h cycling world record: a case study. *J Appl Physiol* 89:1522–1527
4. Defraeye T, Blocken B, Koninckx E, Hespel P, Carmeliet J (2010) Aerodynamic study of different cyclist positions: CFD analysis and full-scale wind-tunnel tests. *J Biomech* 43(7):1262–1268
5. Crouch TN, Burton D, Brown NAT, Thomson MC, Sheridan J (2014) Flow topology in the wake of a cyclist and its effect on aerodynamic drag. *J Fluid Mech* 748:5–35
6. Fintelman DM, Sterling M, Hemida H, Li FX (2014) The effect of crosswinds on cyclists: an experimental study. *Procedia Eng* 72:720–725
7. Fintelman DM, Hemida H, Sterling M, Li FX (2015) CFD simulations of the flow around a cyclist subjected to crosswinds. *J Wind Eng Aerodyn* 144:31–41
8. Crouch TN, Burton D, Thompson MC, Brown NAT, Sheridan J (2016) Dynamic leg-motion and its effect on the aerodynamic performance of cyclists. *J Fluid Struct* 65:121–137
9. Blocken B, van Druenen T, Toparlar Y, Andrianne T (2018) Aerodynamic analysis of different cyclist hill descent positions. *J Wind Eng Ind Aerodyn* 181:27–45
10. Lukes RA, Chin SB, Haake SJ (2005) The understanding and development of cycling aerodynamics. *Sports Eng* 8:59–74
11. Kyle CR (1979) Reduction of wind resistance and power output of racing cyclists and runners travelling in groups. *Ergonomics* 22(4):387–397
12. Zdravkovich MM, Ashcroft MW, Chisholm SJ, Hicks N (1996) Effect of cyclist's posture and vicinity of another cyclist on

- aerodynamic drag. In: Haake S (ed) *The engineering of sport*. Balkema, Rotterdam, pp 21–28
13. Martin JC, Milliken DL, Cobb JE, McFadden KL, Coggan AR (1998) Validation of a mathematical model for road cycling power. *J Appl Biomech* 14:276–291
 14. Iniguez-de-la-Torre A, Iniguez J (2009) Aerodynamics of a cycling team in a time trial: does the cyclist at the front benefit? *Eur J Phys* 30:1365–1369
 15. Defraeye T, Blocken B, Koninckx E, Hespel P, Verboven P, Nicolai B, Carmeliet J (2014) Cyclist drag in team pursuit: influence of cyclist sequence, stature, and arm spacing. *J Biomech Eng* 136(1):011005
 16. Blocken B, Defraeye T, Koninckx E, Carmeliet J, Hespel P (2013) CFD simulations of the aerodynamic drag of two drafting cyclists. *Comput Fluids* 71:435–445
 17. Belloli M, Giappino S, Robustelli F, Somaschini C (2016) Drafting effect in cycling: investigation by wind tunnel tests. *Procedia Eng* 147:38–43
 18. Barry N, Burton D, Sheridan J, Thompson M, Brown NAT (2015) Aerodynamic drag interactions between cyclists in a team pursuit. *Sports Eng* 18(2):93–103
 19. Blocken B, Toparlar Y, Andrianne T (2018) Aerodynamic drag in cycling team time trials. *J Wind Eng Ind Aerodyn* 182:128–145
 20. Blocken B, van Druenen T, Toparlar Y, Malizia F, Mannion P, Andrianne T, Marchal T, Maas GJ, Diepens J (2018) Aerodynamic drag in cycling pelotons: new insights by CFD simulation and wind tunnel testing. *J Wind Eng Ind Aerodyn* 179:319–337
 21. Vogt S, Roecker K, Schumacher YO, Pottgiesser T, Dickhuth H-H, Schmid A, Heinrich L (2008) Cadence-power-relationship during decisive mountain ascents at the tour de France. *Int J Sports Med* 29:244–250
 22. Mognoni P, Di Prampero PE (2003) Gear, inertial work and road slopes as determinants of biomechanics in cycling. *Eur J Appl Physiol* 90(3–4):372–376
 23. Ouvrard T, Gros Lambert A, Ravier G, Grosprêtre S, Gimenez P, Grappe F (2018) Mechanisms of performance improvements due to a leading teammate during uphill cycling. *Int J Sports Physiol Perform* 13:1–25
 24. Foster C, Snyder AC, Thompson NN, Green MA, Foley M, Schragger M (1993) Effect of pacing strategy on cycle time trial performance. *Med Sci Sports Exerc* 25(3):383–388
 25. Atkinson G, Brunskill A (2000) Pacing strategies during a cycling time trial with simulated headwinds and tailwinds. *Ergonomics* 43(10):1449–1460
 26. Abbiss CR, Laursen PB (2008) Describing and understanding pacing strategies during athletic competition. *Sports Med* 38(3):239–252
 27. Wells M, Atkinson G, Marwood S (2013) Effects of magnitude and frequency of variations in external power output on simulated cycling time-trial performance. *J Sports Sci* 31:1639–1646
 28. Wells M, Marwood S (2016) Effects of power variation on cycle performance during simulated hilly time-trials. *Eur J Sport Sci* 16(8):912–918
 29. Wilson DG (2004) *Bicycling Science*. MIT Press, Cambridge, MA
 30. Eindhoven University of Technology (2017) You Tube channel, Wind tunnel movie. https://www.youtube.com/watch?v=VEDn_IUJQfs. Accessed 14 Dec 2020
 31. Artec Europe, Artec Eva, 3D scanners, (2017). <https://www.artec3d.com/3d-scanner/artec-eva>. Accessed 12 Nov 2020
 32. Barlow JB, Rae WH, Pope A (1999) *Low-speed wind tunnel testing*, 3rd edn. Wiley, New York
 33. Franke J, Hellsten A, Schlünzen H, Carissimo B (2007) Best practice guideline for the CFD simulation of flows in the urban environment, COST action 732, quality assurance and improvement of microscale meteorological models
 34. Tominaga Y, Mochida A, Yoshie R, Kataoka H, Nozu T, Yoshikawa M, Shirasawa T (2008) AIJ guidelines for practical applications of CFD to pedestrian wind environment around buildings. *J Wind Eng Ind Aerodyn* 96(10–11):1749–1761
 35. Mannion P, Toparlar Y, Blocken B, Hajdukiewicz M, Andrianne T, Clifford E (2018) Improving CFD prediction of drag on paralympic tandem athletes: influence of grid resolution and turbulence model. *Sports Eng* 21(2):123–135
 36. Blocken B, Malizia F, van Druenen T, Gillmeier SG (2020) Aerodynamic benefits for a cyclist by drafting behind a motorcycle. *Sports Eng* 23:19
 37. ANSYS Inc (2018) *ANSYS fluent—theory guide* 192. ANSYS Inc
 38. Menter FR, Langtry RB, Likki SR, Suzen YB, Huang PG, Völker S (2006) A correlation-based transition model using local variables—part I: model formulation. *J Turbomach* 128(3):413–422
 39. Menter FR, Langtry R, Völker S (2006) Transition modelling for general purpose CFD codes. *Flow Turbul Combust* 77(1–4):277–303
 40. Menter FR, Egorov Y (2010) The scale-adaptive simulation method for unsteady turbulent flow predictions. Part 1: theory and model description. *Flow Turbul Combust* 85(1):113–138
 41. Egorov Y, Menter FR, Lechner R, Cokljat D (2010) The scale-adaptive simulation method for unsteady turbulent flow predictions. Part 2: application to complex flows. *Flow Turbul Combust* 85(1):139–165
 42. Menter F (1997) Eddy viscosity transport equations and their relation to the $k-\epsilon$ model. *J Fluids Eng* 119:876–884
 43. Fröhlich J, von Terzi D (2008) Hybrid LES/RANS methods for the simulation of turbulent flows. *Prog Aerosp Sci* 44(5):349–377
 44. Blocken B, Toparlar Y (2015) A following car influences cyclist drag: CFD simulations and wind tunnel measurements. *J Wind Eng Ind Aerodyn* 145:178–186
 45. Blocken B, Toparlar Y, Andrianne T (2016) Aerodynamic benefit for a cyclist by a following motorcycle. *J Wind Eng Ind Aerodyn* 155:1–10
 46. Le Tour de France (2015) The 80th time at Col du Tourmalet. Retrieved from <https://www.letour.fr/en/news/2015/stage-11/the-80th-time-at-col-du-tourmalet>. Accessed 12 Jan 2021
 47. Long J (2019) Thibaut Pinot sets new Strava KoM on the Tourmalet at the Tour de France 2019. *Cycling weekly*. Retrieved from <https://www.cyclingweekly.com/news/racing/tour-de-france/thibaut-pinot-sets-new-strava-kom-tourmalet-tour-de-france-2019-432124>. Accessed 12 Jan 2021
 48. Marcora SM, Staiano W (2010) The limit to exercise tolerance in humans: mind over muscle? *Eur J Appl Physiol* 109(4):763–770
 49. Tucker R (2009) The anticipatory regulation of performance: the physiological basis for pacing strategies and the development of a perception-based model for exercise performance. *Br J Sports Med* 43(6):392–400
 50. Baron B, Moullan F, Deruelle F, Noakes TD (2011) The role of emotions on pacing strategies and performance in middle and long duration sport events. *Br J Sports Med* 45(6):511–517

Publisher's Note Springer Nature remains neutral with regard to jurisdictional claims in published maps and institutional affiliations.